Kinetics of Phase Segregation: A Review of Some Recent Results*

INTRODUCTION

The terms nucleation, spinodal decomposition, coarsening, Ostwald ripening and Smoluchowski coagulation have all been used to refer to phase segregation processes occuring when alloys, liquid and glassy mixtures, protein solutions, etc., are very rapidly cooled, i.e., quenched, from a high temperature homogeneous state to a temperature where the equilibrium state is one of coexistence of two phases with different compositions. Since there is no time during the quench for the slow diffusion controlled process of spatial segregation to take place, the system finds itself after the quench in a homogeneous nonequilibrium state. It will then undergo an evolution towards the phase segregated equilibrium state specified by the temperature of the bath with which other parameters of the system, e.g., the kinetic energy of the atoms, have come to equilibrium "instantaneously" during the quench. (Other clever methods, e.g., a sudden pressure change, have been used to bring about a similar homogeneous nonequilibrium state in some binary fluid mixtures.) In this Comment we review some findings on these processes obtained from computer simulations on simplified models of AB alloys, e.g., Al–Zn, and relate them to experimental observations.

*Supported in part by NSF Grant DMR81-14726 and by DOE Contract DE-AC02-76ERO3077.

Comments Solid State Phys.
1983, Vol. 10, No. 6, pp. 201–217
0308-1206/83/1006-0201/$18.50/0

THEORY

The theoretical analysis of the phase segregation processes in alloys generally deals either with (a), the evolution of the structure function $S(\mathbf{k},t)$ or (b), the grain distribution $c(l,t)$; t is the time after quenching, $\mathbf{k}$ is a reciprocal wave vector, and l is the grain size. This division corresponds to the two principal experimental methods of study: x-ray or neutron scattering and electron microscopy. We shall refer broadly to these as Cahn–Hilliard and Becker–Döring types of theories, respectively.

(a) The Cahn–Hilliard type of theory[1,2] assumes that although the system is undergoing an irreversible process during coarsening, it may be described by a free energy of the form

$$F = \int \left[f(n) + \frac{1}{2} K(\nabla n)^2 \right] d\mathbf{r}. \tag{2.1}$$

Here $n = n(\mathbf{r},t)$ is the local composition variable (fractional concentration of A atoms less that of B atoms) at position $\mathbf{r}$ at time t and $f(n)$ is a local free energy density which, for temperatures below T_c, has two distinct minima at values of n in the two coexisting equilibrium phases. The term $\frac{1}{2}K(\nabla n)^2$ with $K > 0$ is the contribution to the free energy density from the nonuniformity of the system. The (variational) derivative of F with respect to $n(\mathbf{r},t)$ gives rise to a local chemical potential whose gradient is the driving force for phase segregation.

These ingredients lead to a nonlinear kinetic equation for $n(\mathbf{r},t)$ whose linearization around $\bar{n}$, the average composition of the system, gives a simple expression for the early time evolution of $S(\mathbf{k},t)$ (when deviations from uniformity are small):

$$\begin{aligned} S(\mathbf{k},t) &\simeq S(\mathbf{k},0) \exp\,[2R(k)t], \\ R(k) &\equiv -Mk^2[\partial^2 f(\bar{n})/\partial \bar{n}^2 + Kk^2], \end{aligned} \tag{2.2}$$

where $M > 0$.

Using (2.2) we may distinguish two regions inside the coexistence curve: a *spinodal region* where $\partial^2 f(\bar{n})/\partial \bar{n}^2 < 0$ and a *metastable region* where $\partial^2 f/\partial \bar{n}^2 > 0$ (see Figure 1). If the quench is to the spinodal region the system is unstable with respect to weak long-wavelength fluctuations [$R(k) > 0$] and the growth of these fluctuations into zones of the coexisting phase is then known as *spinodal decomposition*. In the metastable region the system is stable with respect to small fluctuations, but will still be unstable with respect to strong localized fluctuations (i.e., nucleus formation). Phase separation then requires some extra activation energy and is said to be a consequence of the *nucleation* mechanism.

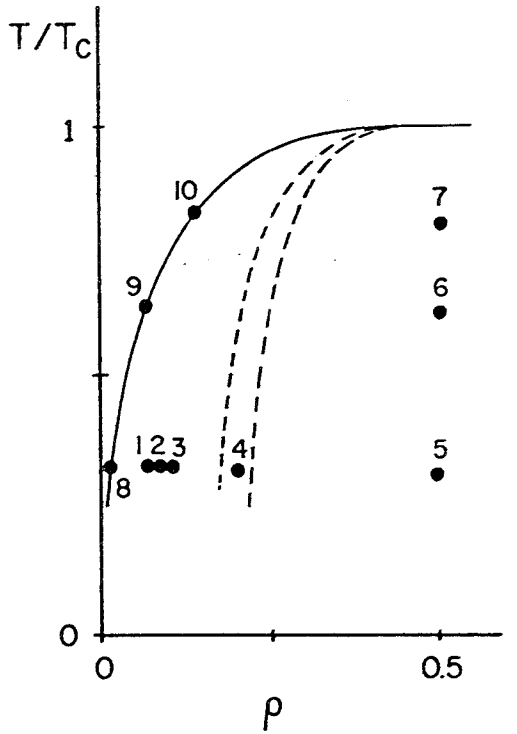

FIGURE 1 Temperature-density section of the phase diagram corresponding to the infinite three-dimensional binary alloy (or Ising) model. The coexistence curve (full line) is drawn according to a low-temperature series expansion and a (5/16) law near $T_c \simeq 4J/0.88686\,k_B$. The broken lines are classical (mean-field theory) spinodals, supposed boundary between metastable and unstable states, according to different assumptions about the local free energy density. The text refers to data corresponding to the quench of the (finite) model system described in Section 3 from an infinite temperature state to the phase points P_j, j = 1–10. The phase points P_1–P_5 are characterized by $T = 8J/3k_B \simeq 0.59\,T_c$ and ρ = 0.05, 0.075, 0.1, 0.2 and 0.5 respectively. P_6 and P_7 (both at ρ = 0.5) correspond to $T = 4J/1.137\,k_B \simeq 0.78\,T_c$ and $T = 4J/k_B \simeq 0.89\,T_c$ respectively. P_8–P_{10} are at the coexistence curve at $T \simeq 0.59\,T_c$, $0.78\,T_c$ and $0.89\,T_c$ (where ρ = 0.01456, 0.0613 and 0.12463, respectively).

While the above simple picture provides good insight into the phenomena of interest, it is inadequate to describe the experimental data.

The latter generally show a less clear distinction (if any) between unstable and metastable regions, a slower than exponential growth of $S(\mathbf{k},t)$ and a decrease in the location of the peak of $S(\mathbf{k},t)$, $k_{max}(t)$, with time (corresponding to an increase in the dimensions of the phase separated regions). Further analysis[3] has shown that nonlinear effects account for some but not all of the discrepancies with experiment.

One of the conceptual problems of the Cahn–Hilliard type of theory concerns the meaning of the local free energy functional $f(n)$ (first introduced by van der Waals and Gibbs) with its regions of negative curvature. As is well known, such a form cannot be derived from equilibrium theory without the addition of extra constraints. The correct formulation of such constraints and the derivation of an appropriate free energy based on them still requires more work.

(b) The Becker–Döring types of theories[4,5] are simplest to consider when the composition $\bar{n}$ is close to the coexistence curve with a low concentration of A atoms. They then describe the state of the system as a collection of well separated, more or less spherical, grains of the minority A-rich phase. The coarsening is then expected to proceed predominantly by single atom processes where larger grains grow at the expense of smaller ones, which tend to be dissolved. This is the mechanism known as *Ostwald ripening*. Using macroscopic concepts, this theory predicts that the mean volume of the grains will grow linearly in time: $\lambda^3(t) = \lambda_0^3 + \text{const} \times t$ where $\lambda(t)$ is the mean radius at time t after quenching. In situations where the grains are not so well separated the coarsening may proceed by effective diffusion and coagulation of clusters of solute atoms, the so-called *Smoluchowski coagulation*. Simple dimensional arguments then lead to the prediction $\lambda \sim t^{1/6}$.

These considerations are also relevant for analyzing the structure function from scattering experiments. Assuming that the location of the peak of $S(\mathbf{k},t)$ is a measure of the characteristic length λ gives $k_{max} \sim \sqrt{\lambda(t)}$. Again it is difficult to assess the validity of the assumptions in the grain dynamics approaches or to make more quantitative predictions, and a more complete theory is highly desirable.

COMPUTER SIMULATIONS

The model used in our simulations consists of a simple cubic lattice with periodic boundary conditions whose N sites (N = 27 000 or 125 000) are occupied by either A or B particles; at each site i, $n_i = \pm 1$, respectively. The two possibilities can also be interpreted as being an occupied or an empty site, or as being an "up" or "down" Ising spin. There is a "ferromagnetic" interaction between nearest-neighbor sites:

$$E = -J \sum_{n.n.} n_i n_j, \qquad J > 0, \tag{3.1}$$

favoring segregation into an A-rich and a B-rich phase. This gives rise in the infinite system to a symmetric coexistence curve whose shape is numerically well known.

In the simulations the kinetics of the system is represented by "Kawasaki dynamics," a Markov process whose basic step is the interchange of an A and a B atom on nearest neighbor sites with a probability $\exp(-\beta\Delta E_{ij})/[1 + \exp(-\beta\Delta E_{ij})]$, where $\beta = 1/k_B T$, T is the temperature of quenching and ΔE_{ij} is the change in energy resulting from the interchange. This procedure assures that the system will reach asymptotically a canonical equilibrium state with the average fraction of solute, A, atoms, $\rho = (\bar{n} + 1)/2$, $0 \leq \rho \leq 1$ remaining constant in time. The rate at which a given bond is picked for a possible exchange is $(1/3)\alpha$; α^{-1} is our unit of time.

RESULTS FROM COMPUTER SIMULATIONS

The dots in Figure 1, labeled 1 to 10, represent density-temperature points P_j to which the model alloy was quenched from an initial random configuration corresponding to an infinite temperature; they are defined in the caption for Figure 1 and in Table 1.

Structure Function

A quantity of primary interest in the simulation was the structure function $S(\mathbf{k},t)$ which is defined here

$$S(\mathbf{k},t) = N^{-1} \sum_{\mathbf{r}} e^{i\mathbf{k}\cdot\mathbf{r}} \sum_{l} \Big\langle [n(\mathbf{r}_l,t) - \bar{n}]\,[n(\mathbf{r}_l + \mathbf{r},t) - \bar{n}] \Big\rangle, \tag{4.1}$$

TABLE I

Values of the adjustable parameters assuming a linear behavior of k_1^{-3} with time using the data for $t \geq t_0$

Phase point		Maximum duration of run	L	NR	$k_1^{-3} = A + Bt/10^3$, $t \geq t_0$ A	B	t_0	$k_1 \sim t^{-a}$ a
P_1	0.59 T_c 5%	14 000	50	1	8.8	1.5	6800	0.35
P_2	0.59 T_c 7.5%	10 200	50	1	7.5	1.5	4000	0.23
P_3	0.59 T_c 10%	7 300	50	1	3.6	1.5	2500	0.21
P_4	0.59 T_c 20%	3 900	30	8	2.3	1.7	1500	0.19
P_5	0.59 T_c 50%	650	30	8	1.2	3.0	350	0.19
P_6	0.78 T_c 50%	1 700	30	8	1.4	3.9	1000	0.23
P_7	0.89 T_c 50%	6 600	30	8	3.5	3.9	1000	0.25

t_0 is the approximate time at which we observed the onset of the dynamic scaling of the structure function according to Eq. (4.6). The values of the exponent obtained assuming a simple power law behavior are also shown (here all the data except the very early one are included in the fit). L refers to the size of the system, and NR is the number of independent runs made at that particular phase point.

where $n(\mathbf{r}_i) \equiv n_i$, $\mathbf{r}$ and $\mathbf{r}_i$ run over the N lattice sites and $k = (2\pi/L)\mu$, $\mu_\alpha = 0, \pm 1, \ldots, \pm L/2 (\alpha = 1,2,3)$, $L = N^{1/3}$, is in the first Brillouin zone. The $< >$ represents an ensemble average which could in principle be implemented on the computer by making many independent runs. (In practice we used between one and eight independent runs—see Table I—and relied on the spatial averaging given in (4.1) as well as on an average over various time intervals.) According to the definition (4.1), $S(\mathbf{k} = 0,t) = 0$, $N^{-1} \Sigma_{\mathbf{k}} S(\mathbf{k},t) = (1 - \bar{n}^2)$, and $S(\mathbf{k},0) \simeq (1 - \bar{n}^2)$, $\mathbf{k} \neq 0$, corresponding to the initial random configuration.

We consider a "spherically" averaged structure function $S(k,t)$ depending only on the wave number $k \equiv 2\pi\mu/L$, $\mu = 0,1, \ldots, \sqrt{3}\, L/2$, obtained by averaging $S(\mathbf{k},t)$ over all values of $\mathbf{k}$ in the first octant, $k_\alpha \geq 0$, $\alpha = 1,2,3$, such that

$$(2\pi/L)\,(\mu - \tfrac{1}{2}) \leq |\mathbf{k}| < (2\pi/L)\,(\mu + \tfrac{1}{2}).$$

In our simulations we were able to monitor $S(k,t)$ for 10 shells, $\mu = 1, \ldots, 10$, for the $L = 30$ lattice used at points P_4 to P_7 and for 14 shells in the $L = 50$ lattice used for P_1 to P_3 and for P_8 to P_{10}.

Figure 2 shows plots of $S(k,t)/(1 - \bar{n}^2)$ versus k at different times for a quench to P_5. The plots for other points inside the miscibility gap

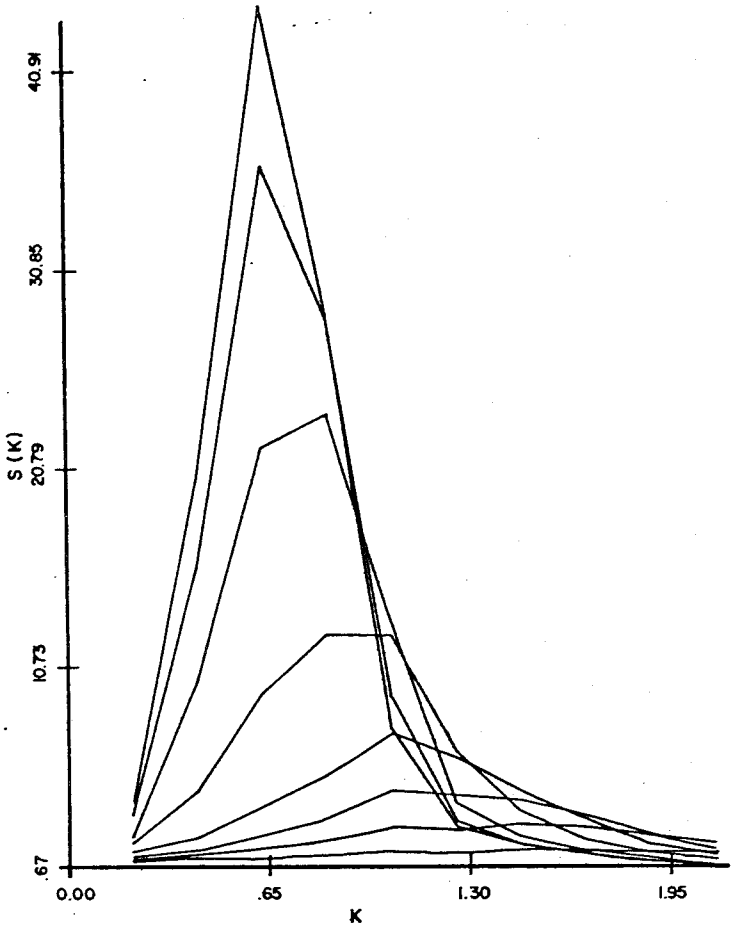

FIGURE 2 $\bar{S}(k,t) = S(k,t)/(1 - \bar{n}^2)$ vs k (in units of the lattice spacing) for the quench to the phase point P_5 (deep quench). Increasing values of time, in units of attempted interchanges per site, correspond to the different graphs from the bottom of the picture to the top.

are qualitatively similar.[6] A different behavior of $S(k,t)$ occurs when the system is quenched to the points P_8–P_{10} at or outside the coexistence curve. In those cases, $S(k,t)$ rapidly approaches a common envelope which has the Ornstein–Zernike form $S(k) \sim (\xi^2 + k^2)^{-1}$.

A comparison of the behavior for points P_1 to P_5 shows[7] that the speed of the segregation increases rapidly, in units of α^{-1}, with the distance of the quench from the coexistence line. The same is true for the points P_5 to P_7. This accounts, in the main, for the widely different time lengths to which we ran our simulations (Table I). It is clear that close enough to the coexistence line at $T \simeq 0.6\, T_c$, the relaxation time would become so long that the system would appear, for all practical purposes, to be in a metastable state, while close to T_c the system will be in the region of critical slowing down. In either case the segregation would not be visible in the simulations.

While there is no evidence in the simulations of any *abrupt* change in the kinetics on crossing any spinodal line, there are some differences in the way in which $S(k,t)$ evolves with time in different parts of the coexistence region. For quenches deep in the coexistence region $S(k,t)$, for fixed k, decreases strongly after reaching its maximum value while near the coexistence line it remains approximately constant for the times observed. This behavior results in the crossovers at large k seen in $S(k,t)$ versus k curves in Figure 2 which do not occur, say for P_1. Such crossovers have been conjectured to be the hallmark of quenches inside the spinodal curve.

Scaling

Experiments and theory always deal with macroscopic size systems which correspond in the model to $N \to \infty$, k becoming a continuous variable and $S(k,t)$ a continuous function of k. Let $\mathcal{S}(k,t)$ be the limit of $S(k,t)$ as $N \to \infty$ and $\mathcal{S}_{eq}(k)$ be the equilibrium structure function of a macroscopic system fully segregated into two pure phases, i.e., the expected limit of $\mathcal{S}(k,t)$ as $t \to \infty$. This has the form

$$\mathcal{S}_{eq}(k) = (\bar{n}_0^2 - \bar{n}^2)\bar{\delta}(k) + \mathcal{S}_{coex}(k;T), \tag{4.2}$$

where $\bar{\delta}(k)$ is the sphericalized Dirac delta function at $k = 0$, $\bar{n}_0(T)$ is equal to $\bar{n}$ on the coexistence line and $\mathcal{S}_{coex}(k;T)$ is the equilibrium structure function on that line. This suggests that a useful quantity for analysis in our small system, i.e., one that will more clearly reveal the essential features of the coarsening process in macroscopic systems, is

$$S_1(k,t) \equiv [S(k,t) - S_{coex}(k;T)]\,(\bar{n}_0^2 - \bar{n}^2)^{-1}. \tag{4.3}$$

The function $S_{coex}(k;T)$ (which is the same for both pure phases by the symmetry of the model) was obtained for the three different temperatures T considered here by quenching to the points P_8, P_9 and P_{10} on the coexistence line and waiting for the system to reach equilibrium. It was then conjectured that the function $\mathcal{S}_1(k,t)$ may be related at late times to a scaled function $\mathcal{F}$ such that

$$\mathcal{S}_1(k,t) \simeq b(t)\, \mathcal{F}(k/K(t)), \tag{4.4}$$

where $K(t)$ is some characteristic wave vector in the system. Remembering that the sum over k in (4.1) is time independent, we set $b(t) = 2\pi^2 K^{-3}$ so that

$$\int_0^\infty x^2 \mathcal{F}(x)dx = 1. \tag{4.5}$$

To test the extent of scaling and find $\mathcal{F}(x)$ from our simulations we defined a function of two variables, $x = k/k_1(t)$ and t, by the relation

$$F(x;t) \equiv \frac{(L/\pi)\, k_1^3\,(t) S_1(xk_1(t),t)}{\sum_{k=0}^{\kappa} k^2 S_1(k,t)}, \tag{4.6}$$

where $\kappa \simeq 0.55\pi$ (i.e., we dropped the last two shells for $L = 30$), and then looked whether for late times $F(x;t) \simeq F(x)$, a smooth function of x independent of t. This was in fact what we found.

The values of $F(x;t) \simeq F(x)$ independent of t, obtained from the simulations for large times are shown (along with real experimental data; see figure caption) in Figure 3 in the case of the quenches to P_4, P_5 and P_6. While the curves obtained in this way for "deep" (P_4–P_6), "intermediate" (P_3) and "shallow" (P_1, P_2 and P_7) quenches are all similar, the scatter of the data within each group is significantly smaller than between them.[7] We believe therefore that there is a real, albeit

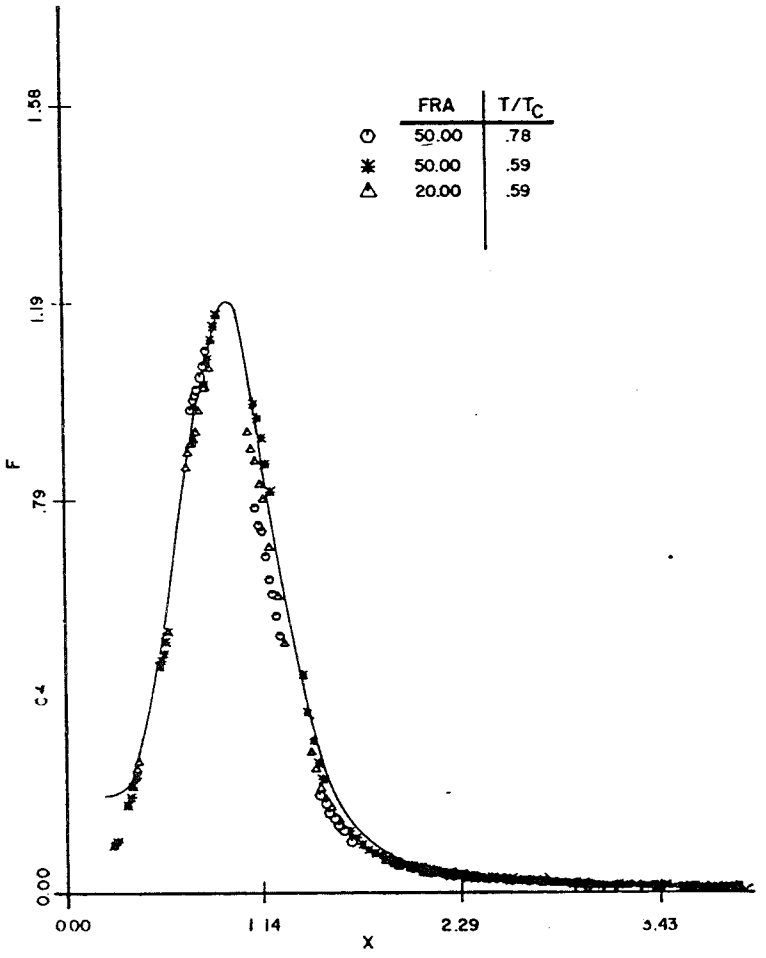

FIGURE 3 The scaling function $F(x;t)$ defined in Eq. (4.6) is plotted here vs $x = k/k_1(t)$. This figure compares data from the computer simulation (symbols) with the experimental data in Figure 3 of Ref. 14 (full line) corresponding to Au-60 at.% Pt alloy quenched to $T \simeq 0.6\ T_c$. Only the vertical scale was adjusted to obtain the present fit. The asterisks correspond to the simulation at P_5 (they represent all the data for $t \geq 350\ \alpha^{-1}$), the triangles are for P_4 (representing all the data for $t \geq 1500\ \alpha^{-1}$), and the circles correspond to the quench to P_6 ($t \geq 1000\ \alpha^{-1}$).

small, difference between the scaling function $F(x)$ at different quenches. This change in the scaling function may perhaps be explained by the difference in the boundaries of the single phase regions changing from smooth to corrugated as we get closer to the critical point. The similarity of $F(x)$ near T_c and near the coexistence curve for small ρ would appear to suggest some sort of "spinodal line" criticality. This is an intriguing question which is very difficult to answer at present.

We have also performed a fit to F of the form $(\alpha_1 + \alpha_2 x^4)^{-1}$ for $x > x_{max}$, the location of the maximum of $F(x)$, which seems to be suggested by Ref. 8. While this is approximately the behavior of the data for $1 < x \lesssim 2$, it clearly deviates from the x^{-4} behavior at larger x values. This may be due to the fact that the $F(x)$ for $x > 2$, where $F(x) \ll 1$, can be determined only poorly and it does appear that it may converge slowly to x^{-4} for $2 < x < 3$.

Moments

A quantitative feature $S(k,t)$, which can go over smoothly to the macroscopic $\mathcal{S}(k,t)$, is the moments

$$k_m(t) = \langle k^m \rangle = \sum_{k=0}^{\kappa} k^m S_1(k,t) \Big/ \sum_{k=0}^{\kappa} S_1(k,t), \qquad m = 1,2 \quad (4.7)$$

where $\kappa \simeq 0.55\pi$ as before. The analysis of $k_1(t) \sim k_{max}(t)$ according to the predictions $k_1(t) \sim t^{-a}$ shows a slow time dependence of the exponent a which tends to increase with time. Table I lists the a values obtained from a log–log fit to the data excluding only the "very early" times (typically for $t > 200$). Those values, interpreted according to the grain dynamics approaches described in Section 2, suggest that the effective diffusion and coagulation of the grains is the predominant mechanism in the case of deep quenches (e.g., at P_4 and P_5), (and also during the early stages of the evolution at almost any location inside the coexistence line) while single atom processes tend to dominate when the quench is close to the coexistence line (e.g., at P_1 and P_7) late in the evolution. As a matter of fact, the k_1 values corresponding to all the phase points studied seem to follow, after a time t_0 (which marks the onset of the dynamic scaling of the structure function), the Lifshitz–Slyozov prediction that $k_1^{-3} \sim \lambda^3$ evolves linearly in time (Table I).

Cluster Distribution

A *cluster* is defined in our lattice model system as a group of A atoms linked together by nearest-neighbor bonds. At low concentrations of the minority component, large clusters in our model are expected to correspond approximately to the grains observed by microscopy in real materials.

The cluster distribution $c(l,t)$ specifies the total number of clusters of size l at time t after quenching. At P_1 to P_5 the time evolution of $c(l,t)$ seems to follow the general predictions of the Becker–Döring and Lifshitz–Slyozov theory, but detailed comparision with theory is hampered (among other reasons) by: (i) imprecision in the separation between "small" and "large" clusters, the former being part of the vapor phase, (ii) the scarcity and corresponding large fluctuations in the number of large clusters and (iii) lack of knowledge of appropriate rate constants. We shall therefore only describe here some gross features of the cluster distribution as observed in quenches to $T \simeq 0.6\ T_c$; see Refs. 9 for other details.

For values of ρ very close to ρ_s ($\simeq 0.015$), the corresponding saturated vapor density, $c(l,t)$ rapidly settles to a stationary metastable value on the time scale of the computer experiment. At $\rho = 0.05$ the distribution of "small" clusters (say, $1 \lesssim l \lesssim 10$ or so) still approaches rapidly a quasistationary distribution characteristic of metastable states but the size of the large clusters now increases. It does so very slowly up to $t \simeq 2000\ \alpha^{-1}$ but afterwards it increases at a rate comparable to quenches deeper in the coexistence line. It thus seems that it takes some time for the system to find its way out of metastability, a situation which might be related to what experimentalists have described as a "cloud point".[16,18] At $\rho = 0.075$ there is from the beginning a measurable rate at which larger clusters develop, i.e., a finite nucleation rate. As the density is increased further, $\delta \gtrsim 0.1$, we observe the early appearance of relatively large loose clusters ($l \gtrsim 50$) coexisting with very small clusters of size one to ten or so. The number of A atoms and their relative distribution in the small clusters is close to that observed in the A-poor *(gas)* phase equilibrium state. The system then undergoes a slower process in which the larger clusters grow and become more compact. When the density of A atoms is increased further, the system undergoes *percolation*, i.e., the appearance of "infinite" size clusters. Our definition of clusters is then useless and if the concept is to remain meaningful a new definition which considers not only the size but also the shapes, composition and distribution of the clusters is required. Just how well this can be done in a microscopic lattice theory is still an open question.

COMPARISON WITH EXPERIMENTS

The model used in the simulations certainly involves a great oversimplification of the behavior of real materials. Despite this, the simulation results are frequently very similar to experimental observations. For example, the location and height of the peak of the scattered intensity in the classical experiment by Rundman and Hilliard[10] on an aluminum–zinc alloy at 423°K ($\simeq 0.7\ T_c$) can be *roughly* characterized by the simple power laws $k_{max}(t) \sim t^{-a}$ and $S(k_{max}(t),t) \sim t^{3a}$ respectively with $a \sim 0.2$–0.23, values roughly consistent with those found for the model system quenched to P_4.

In comparisons with real experiments, attention must be paid to the relation between the units and other characteristics of the model and those corresponding to actual materials. To get at least a crude idea of how to compare time scales, we note that the diffusion coefficient of a single A atom in the model system filled with B atoms is $D = \alpha/6$, since the probability that a given bond will be tried in time dt is $(1/3)\alpha dt$ and if tried, the probability of an exchange is $\frac{1}{2}$. We therefore think of $\alpha^{-1}(T)$ as roughly comparable to $a_0^2/6\ D_0(T)$ where a_0 is the lattice spacing and $D_0(T)$ is the diffusion constant of a real alloy at temperature T in the limit of zero concentration of A atoms. The lattice spacing a_0 is the unit of length in the model. The relevant parameters for the Al–Zn alloys are estimated to be $a_0 \simeq 3$ Å, $T_c \simeq 350$°C and $D_0 \sim 10^{-18}$ cm^{2}s^{-1} at $T = 0.6\ T_c$. According to this estimate, $\alpha^{-1} \sim 50$ s at $0.6\ T_c$ and the physical time interval in our studies at P_1 to P_5 is many hours. A similar estimate at $0.8\ T_c$ gives $\alpha^{-1} \sim 10^{-4}$ s. While these are at best only order of magnitude computations, it seems that our simulations at $0.6\ T_c$ can be compared with experimental observations on real alloys (where the system relaxation is typically followed for some hours) while one has to be cautious at higher temperatures. We also note that the smallest grains measured in typical experiments contain between 30 and 150 atoms, and the largest ones about 3×10^5 atoms, while the largest clusters observed in our simulations at P_1–P_3 contain no more than 800 A atoms.

Other possible causes of differences between the behavior of the model and experimental observations can be found in the quenching rate, which is finite in real experiments but infinite in the simulations. We have checked that the quenching process may influence the subsequent evolution. For instance, we have been able to reproduce qualitatively the "untypical" (with an *initial* increase of $k_{max}(t)$ corresponding to an initial decrease of the mean clusters radius) observations by Allen *et al.*,[11] corresponding to room temperature aging of Al–Zn quenched into ice water from $T \simeq 0.93\ T_c$, by simulating a similar double quenching of our model system. The influence of the quenching process has also been reported in the case of some liquid mixtures[12] and other systems.[13]

Encouraged by this agreement we have done a more quantitative analysis of the data reported by Singhal *et al.*[14] corresponding to the Au-60 at.% Pt alloy. The experiment gives a structure function with a shape quite similar to the one observed in our simulations or in the Rundman–Hilliard experiment on aluminum–zinc, including the characteristic crossovers at that temperature and composition on the tail, $k > k_{max}$. We have also computed the function $F(x,t)$ defined in Eq. (4.6) taking as $S_1(k,t)$ the experimental data in Figure 3 of Ref. 14. We find that the data satisfy the scaling hypothesis in the time range 120 s $\leq t \leq$ 900 s for $x < 1.8$; see Figure 3. The experimental function $F(x)$ is quite similar to the corresponding one in the case of our simulations at P_4, P_5 and P_6. In fact, one can make the data from the actual and computer experiments lie on the same curve merely by rescaling the vertical axis, as seen in Figure 3.

We find[7] a similar agreement between our scaling function $F(x)$ at P_1 and P_2 and the one reported by Guyot *et al.*[15] corresponding to a sample of Al-15 at.% Zn quenched to $T \simeq 0.6\ T_c$. Dynamic scaling also appears to hold for other aluminum–zinc samples studied except, in some cases,[16] for those at very high temperatures where the scattered intensity is far from saturation and a very large incubation time is observed. Guyot and co-workers have also reanalyzed the temporal evolution of the mean grain radius in their experiments by electron microscopy and find[16] that their data are consistent with a Lifshitz–Slyozov behavior, in agreement with the data from our simulations. Thus, it seems that the behavior of real binary alloys and the behavior of the model alloy described in Section 3 are very close to each other, and that the dynamic scaling of the structure function and the linear increase with time of the mean clusters size are two basic features of the phase segregation phenomena at late times.

Recent observations on binary fluid mixtures[12,17,18] report a behavior which is also qualitatively similar to the one shown by our model system (note, however, when making comparisons that the diffusion coefficient is much larger for fluids, 10^{-4}–10^{-6} cm^{2}s^{-1}, than for alloys). In particular, Goldburg *et al.*[12] have found a scaling behavior of $\mathcal{S}(k,t)$ with a function $F(x)$ which looks quite similar to our function. Dynamic scaling with all the above characteristics has also been reported in a quasibinary glass,[13] ^{3}He–^{4}He mixtures and some features occur also in other materials.[19,20] Further experimental and theoretical work is needed to establish the actual range of this kind of universal behavior and develop a more complete theory of the kinetics of phase transitions.

OTHER SYSTEMS

The dynamic scaling of the structure function has also been observed[21] in computer simulations of an ordering model binary alloy described by a Hamiltonian like (3.1) with $J < 0$. This models the kinetics of quenched alloys like Au–Cu which tend to form ordered superlattices at low temperatures. Simulations at a composition $\bar{n} = 0.5$ give evidence that the "staggered" structure function scales as $kt^{1/2}$. This can be understood by assuming that the radius of the ordered domains increases as $t^{1/2}$. The corresponding two-dimensional system behaves in a qualitatively similar way.

Other computer experiments[22] have been carried out on a model system ("metamagnet") with energy

$$E = -J \sum_{n.n.} n_i n_j + \alpha J \sum_{n.n.n.} n_i n_l + \mathcal{H} \sum_i n_i, \quad J < 0. \qquad (6.1)$$

This may model alloys such as Fe–Al which are known to have tricritical points, mixtures of ^{3}He–^{4}He, or chemisorption systems of adatoms on a substrate. Simulations on a two-dimensional system indicate that the sublattice magnetization structure function exhibits early time scaling $S_s(k,t) = t^{2a}F(kt^a)$, with characteristic exponent $a \simeq 0.35$.

Acknowledgments

We thank K. Binder, W. Goldburg and C. Knobler for valuable discussions.

JOEL L. LEBOWITZ
Department of Mathematics and Physics,
Rutgers University, Bush Campus,
New Brunswick, New Jersey 08903

J. MARRO
Depto. de Fisica Teórica y Depto. de Ecuaciones Funcionales,
Universidad de Barcelona,
Diagonal 647,
Barcelona-28, España

M. H. KALOS
Courant Institute of Mathematical Sciences,
New York University, New York 10012

References

1. For early references on experiments and theory see J. W. Cahn, Trans. AIME **242**, 166 (1968).
2. H. E. Cook, Acta Met. **18**, 297 (1970).
3. J. S. Langer, M. Bar-on and H. D. Miller, Phys. Rev. A **11**, 1417 (1975).
4. R. Becker and W. Döring, Ann. Phys. (Leipzig) **24**, 719 (1935).
5. I. M. Lifshitz and V. V. Slyozov, J. Phys. Chem. Solids, **19**, 35 (1961).
6. For a review of the early results from computer experiments, real experiments and theory, see K. Binder, M. Kalos, J. Lebowitz and J. Marro, Adv. Colloid Interface Sci. **10**, 173 (1979).
7. J. Marro, J. Lebowitz and M. Kalos, Phys. Rev. Lett. **43**, 282 (1979); J. Lebowitz, J. Marro and M. Kalos, Acta Met. **30**, 297 (1982).
8. H. Furukawa, Phys. Rev. Lett. **43**, 136 (1979); Phys. Rev. A, 1981.
9. O. Penrose, J. Lebowitz, J. Marro, M. Kalos and A. Sur, J. Stat. Phys. **19**, 243 (1978); A. Buhagiar, Ph.D. Thesis, Open University, Milton Keynes, UK, 1980; O. Penrose *et al.*, to be published.
10. K. B. Rundman and J. E. Hilliard, Acta Met. **15**, 1025 (1967).
11. D. Allen, J. Epperson, V. Gerold, G. Kostorz, S. Messoloras and R. Stewart, Conference on Neutron Scattering. Gatlinburg, Tennessee, June 1976. V. Gerold and J. Kostorz, J. Appl. Cryst. **11**, 376 (1978).
12. J. S. Huang, W. I. Goldburg and A. W. Bjerkaas, Phys. Rev. Lett. **32**, 921 (1974); W. Goldburg *et al.*, J. Chem. Phys. **68** 484 (1978); W. Goldburg, A. J. Schwartz and M. W. Kim, Prog. Theor. Phys. Suppl. **64**, 477 (1978). Y. C. Chou and W. Goldburg, Phys. Rev. A **20**, 2105 (1979).
13. P. Fratzl, private communication; A. Craievich and J. M. Sánchez, 1981 preprint.
14. S. P. Singhal, H. Herman and G. Kostorz, preprint 1978.
15. G. Laslaz and P. Guyot, Acta Met. **25**, 277 (1977); G. Laslaz, P. Guyot and G. Kostorz, preprint.
16. P. Guyot and J. P. Simon, preprint 1981; also private communications.
17. Y. C. Chou and W. I. Goldburg, Phys. Rev. A, February 1981; also private communications.
18. C. M. Knobler and N. C. Wong, preprints 1981; also private communications.
19. M. Tomazawa, R. K. MacCrone and H. Herman, J. Am. Ceram. Soc. **53**, 62 (1970). P. G. de Gennes, J. Chem. Phys. **72**, 4756 (1980). C. Williams, La Recherche, October 1981. M. Delaye, J. I. Clark and G. B. Benedek, Biophys. J. 1981.
20. T. Benda, P. Alpernaud and P. Leiderer, preprint. J. K. Hoffer, L. J. Campbell and R. J. Bartlett, Phys. Rev. Lett. **45**, 912 (1980).
21. M. Phani, J. Lebowitz, M. Kalos and O. Penrose, Phys. Rev. Lett. **45**, 366 (1980); P. Shani, G. Dee, J. D. Gunton, M. Phani, J. Lebowitz and M. Kalos, Phys. Rev. B **24**, 410 (1981).
22. P. Shani and J. D. Gunton, Phys. Rev. Lett. **45**, 369 (1980).